Supplementary material for

Early Neogene foreland of the Zagros, implications for the initial closure of the Neo-Tethys and kinematics of crustal shortening

Mortaza Pirouz[1], Jean-Philippe Avouac[1], Jamshid Hassanzadeh[1], Joseph L. Kirschvink[1] and Abbas Bahroudi[2]

1) Division of Geological and Planetary Sciences, California Institute of Technology, Pasadena, CA 91125, USA. 2) Exploration Department, Mining Engineering Faculty, University College of Engineering, University of Tehran, North Karghar Street, P.O. Box 1439, Tehran 957131, Iran, and Department of Geoscience, University of Calgary, 2500 University Drive NW, Calgary, AB, Canada, T2N 1N4

Corresponding Author: Mortaza Pirouz, Email Address: mpirouz@caltech.edu or mortaza.pirouz@me.com

This includes:

1. Material and Methods
2. Tables S1 and S2
3. Figures S1 to S8

1. Paleomagnetic methods

Samples were collected in stratigraphic sequence either as 2.54 cm diameter cylindrical cores where possible, or in non-magnetic plastic boxes (7 cc volume, from Natsuhara Giken, Ltd., Osaka, Japan), and oriented using standard techniques including both sun and magnetic compass readings where possible. In the laboratory the cores were trimmed into 1 cm high flat-ended discs using non-magnetic saw blades, and the innermost specimens from each core were selected for measurement processes. Soft sediments in the plastic boxes were impregnated with sodium silicate in a magnetically-shielded space, and then removed from the plastic boxes (allowing thermal demagnetization). In view of the heterogeneous magnetic mineralogy, we used a hybrid demagnetization scheme first involving low-temperature cycling to partially unblock viscous magnetic components held in multi-domain magnetite, then removed low-coercivity components with progressive, 3-axis alternating-field demagnetization up to 7 mT. For detail steps of sample preparation and measurements using the protocols of the Rock and Paleomagnetic Instrument Development [RAPID] consortium please see Kirschvink et al., (2008) and (2015). Upon progressive demagnetization of 114 specimens in the eastern sector (Dehmoord section), 79 samples retained their magnetic direction relatively close to the present local field. Of these, 18 samples reached stable endpoints and produced clear arcs on a stereonet, implying the presence of a two-polarity characteristic component (ChRM) of smaller magnitude (Kirschvink, 1980). Of these, 17 specimens did not reach stable end points but moved far from the present local field. In the Shalamzar section, western Zagros, progressive demagnetization of 65 specimens revealed 18 that maintained their magnetic direction as a stable end point, 11 moved slightly, 14 moved far from the present local field, and 22 specimens show good arcs (Figures S1 & S2). Again, few samples reached the stable final point.

Low-temperature cycling in liquid nitrogen and alternating field (AF) demagnetisation removed ca. 20% of NRM intensity in the soft specimens, compared with ca. 10-15% in the consolidated samples (Figure S3). Most of the specimens display a low blocking temperature overprint with directions similar to the recent magnetic field which is removed by weak AF demagnetization and relatively low thermal demagnetisation up to 150°C. Apparently, it is a combination of viscous remanence and presence of goethite which can be formed during surface weathering and carries a recent or present magnetic field direction (Kirschvink et al., 2015). The low temperature component clusters close to the present local field, while the high temperature components fall into two distinct clusters as shown in Figure S4. After tilt correction, inclination of the high temperature components turn into more downward direction in the Dehmoord section, implying the ChRM was occurred before folding, whereas it is opposite in the Shalamzar section. Table S1 shows summary of the present local field, low and high temperature components for both stratigraphic and tilt corrected, following the combined line and plane analysis of McFadden and McElhinny (1988). Samples of both sections are categorized into three groups signifying the quality of demagnetization analysis, based on the linear and planar demagnetisation patterns using a criterion of MAD values of less than 10˚. The first group (81%) contains samples with an ideal demagnetization pattern in the vector endpoint diagram. The second group (16.4%) present clear movement direction and polarity, but the stable end point is absent. The third group (2.6%) are those with poor or unstable demagnetization trajectories.

2. Rock magnetism

To characterize further the magnetic mineralogy, 28 specimens from different lithologies were subjected to non-destructive rock magnetic experiments at Caltech following the RAPID protocols (Rock and Paleomagnetics Instrument Development Consortium, a.k.a., Kirschvink et al., 2008). The suite of experiments starts with the 3-axis alternating field (AF) progressive demagnetization of the NRM in peak fields up to 120 mT. It is followed by the anhysteretic remanent magnetization (ARM) version of the Lowrie-Fuller test for single-domain behavior (Johnson et al., 1975), which involves progressive acquisition of an ARM in peak alternating-field (AF) of 100 mT, with variable DC biasing fields of 0-1 mT, and progressive AF demagnetisation of the maximum ARM. Samples are then given an IRM pulse in a peak field of 100 mT followed by progressive AF demagnetization (up to 450 mT) to provide the ARM Lowrie-Fuller test for the fraction of the NRM with coercivities below 100 mT (Johnson et al., 1975). Finally, the samples were subjected to progressive IRM acquisition experiments up to 980 mT, again followed by progressive AF demagnetisation and DC demagnetization via backfield IRM progressively up to 750 mT.

We followed the general procedure of Lowrie (1990) to identify the magnetic mineral present based on the distinctive coercivity and blocking temperature characteristics of magnetic minerals. For example, hematite is distinguished by coercivities that range above 1 T and a Néel temperature of 670°, and magnetite has coercivities below the 0.3 T and Néel temperature of 580° (Dekkers, 1989). Some results of coercivity spectral analyses for representative samples from different rock units are shown in Figure S5. The IRM/ARM coercivity spectral analysis of Cisowski (1981) (Figure S5, first row) shows the point of intersection between IRM acquisition and demagnetization curve is about 0.45 for most of the samples (Figure S5, first row). According to Cisowski (1981), if the point of intersection is at 0.5 of the SIRM (saturated isothermal remanent magnetization), there is no magnetic interaction. Care must also be taken the Cisowski (1981) investigation is focused on magnetic interaction for single domain particles and same approach might not be applicable to the pseudo single domain particles. Reproducible coercivity spectra with medium distractive field values spreading between 30-50 mT and clear approach to saturation by 300 mT suggests a ferrimagnetic component such as magnetite (Figure S5a), while the lower Bakhtiari and Asmari samples in the Shalamzar section show saturation at peak pulse field of up to 1 T, indicating presence of a high coercivity antiferromagnetic phase like hematite (Figure S5b). ARM acquisition curves plot halfway between the chiton tooth and magnetotactic bacterial reference curves (Figure S5, second row). This shows the presence of a mixture of interacting and non-interacting particles in the Bakhtiari Formation in the Shalamzar section (Figure S5b), while the interacting particles dominate in the Agha Jari and Mishan Formations (Figure S5a), and non-interacting particles in the Asmari Formation (Figure S5b). The Lowrie-Fuller test (Johnson et al., 1975), as shown in the third row of figure S5, reveals magnetic particles are dominated by single domain or pseudo single domain particles. On all samples of Shalamzar section (Figure S5b, third row) the curve for the progressive AF demagnetisation of the ARM lies on top of the IRM curves, whereas some samples from the Dehmoord section (Mishan and Bakhtiari) show that the IRM curve lies above the ARM curve, indicating domination of multi domain particles (Figure S5a, third row). Fuller NRM origin test (Figure S5, last row) compares the intensity of the NRM remaining during AF demagnetization and isothermal remanent

magnetization and illustrates the NRM signal is depositional or post depositional remanent magnetization rather than chemical or thermoremanent magnetization (Fuller et al., 1988). This is because the values are nearly 3 orders of magnitude less than the corresponding IRM levels and nearly 2 orders below the ARM values (Figure S5, last row).

3. Eastern Zagros, Dehmoord (village of *Myrtle* plant) section:

In the eastern sector, Dehmoord section, a pair of reverse and normal polarity intervals between 280-650 m appear to correlate with chrons C6 and C5E, just above the Sr time constraints (Figure S6a & Figure 5a in the main text). Chrons C6 and C5E in the Dehmoord section are reconstructed by 41 samples in which 38 samples (93%) are in quality group 1 (black dots in VGP latitude graph in Figure S6). Chrons C5D, C5C are occupied with large reverse polarity which correlate with 650-1240 m of the section covered with 46 samples in total, 83% in class 1 and 17% in classes 2 and 3 (open dots in VGP latitude graph in Figure S5) (Figure S6a). Two relatively large normal polarity intervals between 650-940 m of the section can be correlated only with the reverse polarities of the C5D and C5C chrons. The lower part of the section, between 40-240 m (Figure 5a), represents mostly thick red marl sediments and thin sandstone and conglomerate interbeds which might have non-linear sedimentation rates. This portion is correlated with C6A and upper part of the C6AA.

4. Western Zagros, Shalamzar (*Tragacanth* grove) section:

In the upper part of the Asmari limestone, the existence of reverse polarity between 20 and 110 m after 34 Ma argues for correlation with C12 chron (Figure S6b and Figure 5b in the main text). The upper part of the Asmari is correlated with C11, which reveals the top of the Asmari Formation has an age of 29 Ma in the western sector. The main part of the foreland deposits are eroded and covered with quaternary deposits, while the Bakhtiari Formation exposes an exceptional outcrop with marine deposits which had been investigated for magnetostratigraphy and Sr ages. Using Sr anchor points let us to correlate the normal polarities in our measurements with the C6B chron (Figure 5b).

Table S1: Paleomagnetic results for the Shalamzar and Dehmoord sections. LT, Low Temperature; PLF, Present Local Field; N, Number of samples; Dec., Declination; Inc., Inclination; κ, Fisher's precision parameter; α9 = 95% confidence cone. *Values have been corrected for the tilt of bedding. Shalamzar is located at 32°N and 50.8°E, and Dehmoord at 29.7°N and 54.1°E.

location	components		N	Dec.	Inc.	κ	α95
Shalamzar	LT≈PLF		62	357.8	46.6	7.95	6.84
	ChRM	Normal lines	30	355.8	56.1	9.25	9.14
		*	30	6.3	32.1	8.41	9.64
		Reverse lines	11	179	-57.8	3.23	29.17
		*	11	191.8	-32.8	3.32	28.62
		Reverse lines & arcs	22	183.4	-53.9	5.68	14.29
		*	22	192.8	-29.9	5.83	14.08
Dehmoord	LT≈PLF		114	358.9	44.4	43.44	2.03
	ChRM	Normal lines	79	359.6	35.7	13.65	4.48
		*	79	0.5	53.7	11.99	4.8
		Reverse lines	18	181.9	14.7	8.28	12.79
		*	18	181.9	-6.7	8.9	12.28
		Reverse lines & arcs	26.5	181.5	9.2	9.28	9.74
		*	26.5	180.7	-11.5	9.82	9.44

Table S2: Measured strontium isotope ratios.

No	Sample	Min. age	Age (Ma)	Max. (age)	$^{87}Sr/^{86}Sr$	Error	Formation	Location (X , Y)	Location
1	Bk1	21.33	**21.46**	21.60	0.708355	0.000001		50.806017° , 32.055933°	
2	Bk2	20.82	**21.01**	21.20	0.708385	0.000002	Bakhtiari	50.806020° , 32.055888°	
3	Bk3	22.46	**22.62**	22.76	0.708276	0.000001		50.805749° , 32.055743°	Shalamzar
4	As1	34.03	**34.29**	34.68	0.707794	0.000003		50.831263° , 32.009455°	
5	As2	34.37	**34.80**	35.57	0.707780	0.000003	Asmari	50.831349° , 32.009576°	
6	As3	34.34	**34.74**	35.49	0.707781	0.000003		50.832567° , 32.011217°	
7	A-J1	26.38	**27.10**	27.80	0.708089	0.000013		54.060843° , 29.773315°	
8	A-J2	27.60	**27.97**	28.27	0.708062	0.000004	Asmari-Jahrom	54.060843° , 29.773315°	
9	A-J3	27.51	**27.91**	28.27	0.708064	0.000006		54.021233° , 29.753200°	
10	Mn1	19.64	**19.73**	19.83	0.708457	0.000001		54.057704° , 29.781983°	Dehmoord
11	MN2	19.97	**20.12**	20.31	0.708431	0.000002		54.057370° , 29.782561°	
12	Mn3	19.84	**19.95**	20.13	0.708441	0.000002	Mishan	54.057370° , 29.782561°	
13	Mn4	21.13	**21.39**	21.63	0.708360	0.000009		54.066716° , 29.762411°	
14	Mn5	19.48	**19.57**	19.67	0.708469	0.000002		54.066570° , 29.762296°	

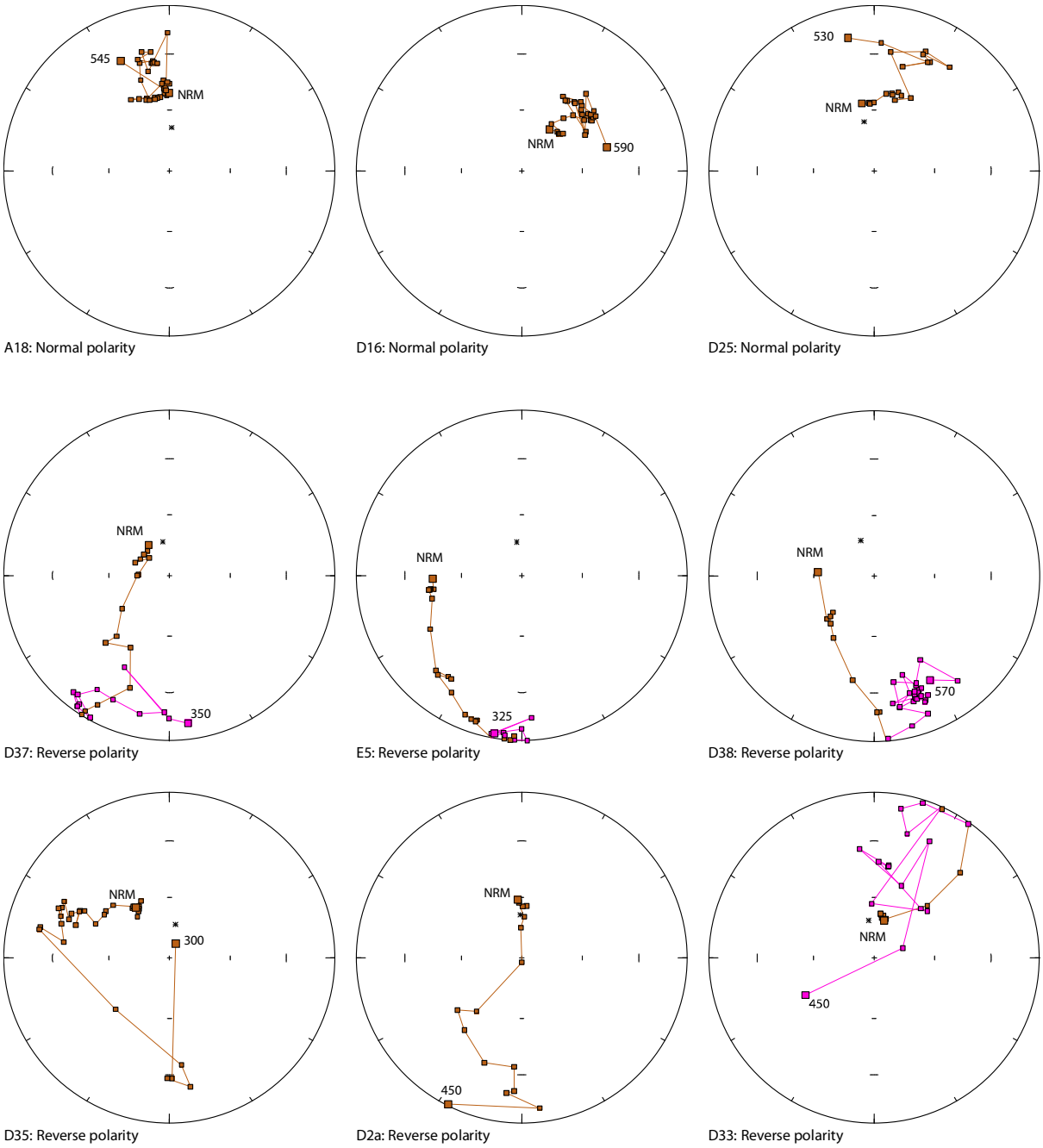

Figure S1: Equal-area projection of various types of paleomagnetic behavior observed for representative samples with normal and reverse polarities. Partial magnetisation stages are shown for each sample; NRM and final thermal stage are highlighted with larger squares.

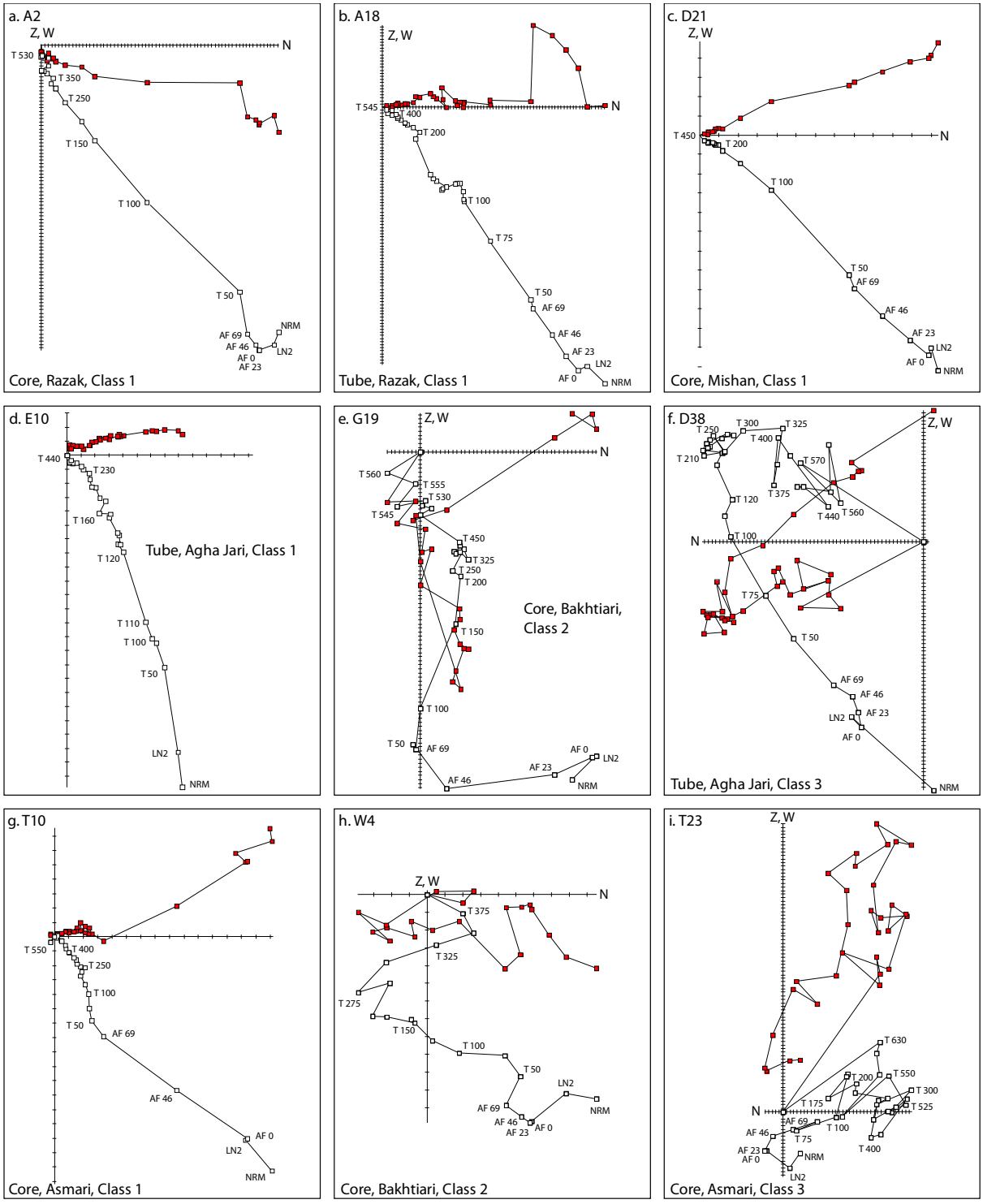

Figure S2: Representative tilt corrected diagrams of thermal demagnetization curves. The red and white squares represent the measured horizontal and vertical projections (Zijderveld, 1967). Specimen names are in the upper left corner. Sample type, lithofacies association and quality of the magnetic directions are also indicated for each panel. The location of the samples are shown in Figure 4. *a* to *f* panels belong to the Dehmoord section, and *g* to *i* panels are for the Shalamzar section.

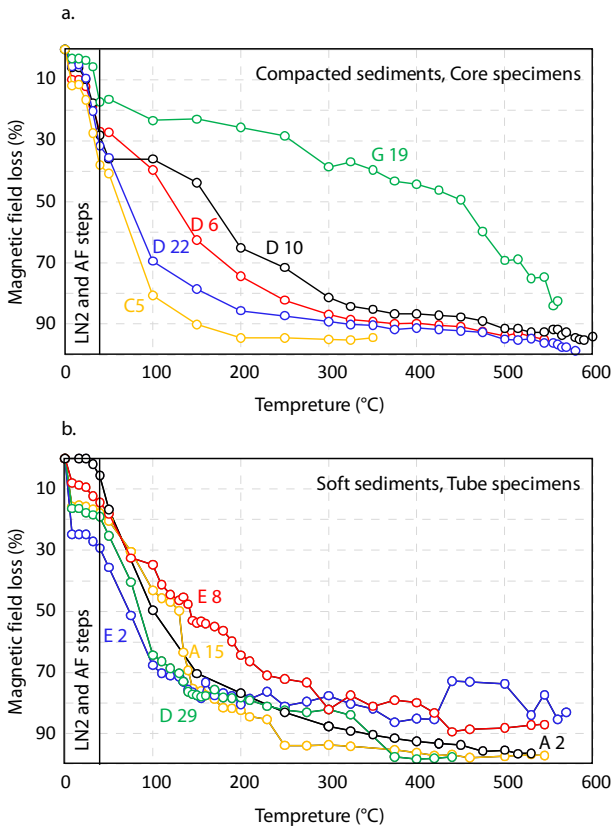

Figure S3: Magnetic field loss of representative core (a) and tube (b) specimens. Some samples obtained magnetic field in the high temperature demagnetization steps (i.g. E2 and E8 tube samples above 420°C) due to formation of secondary minerals.

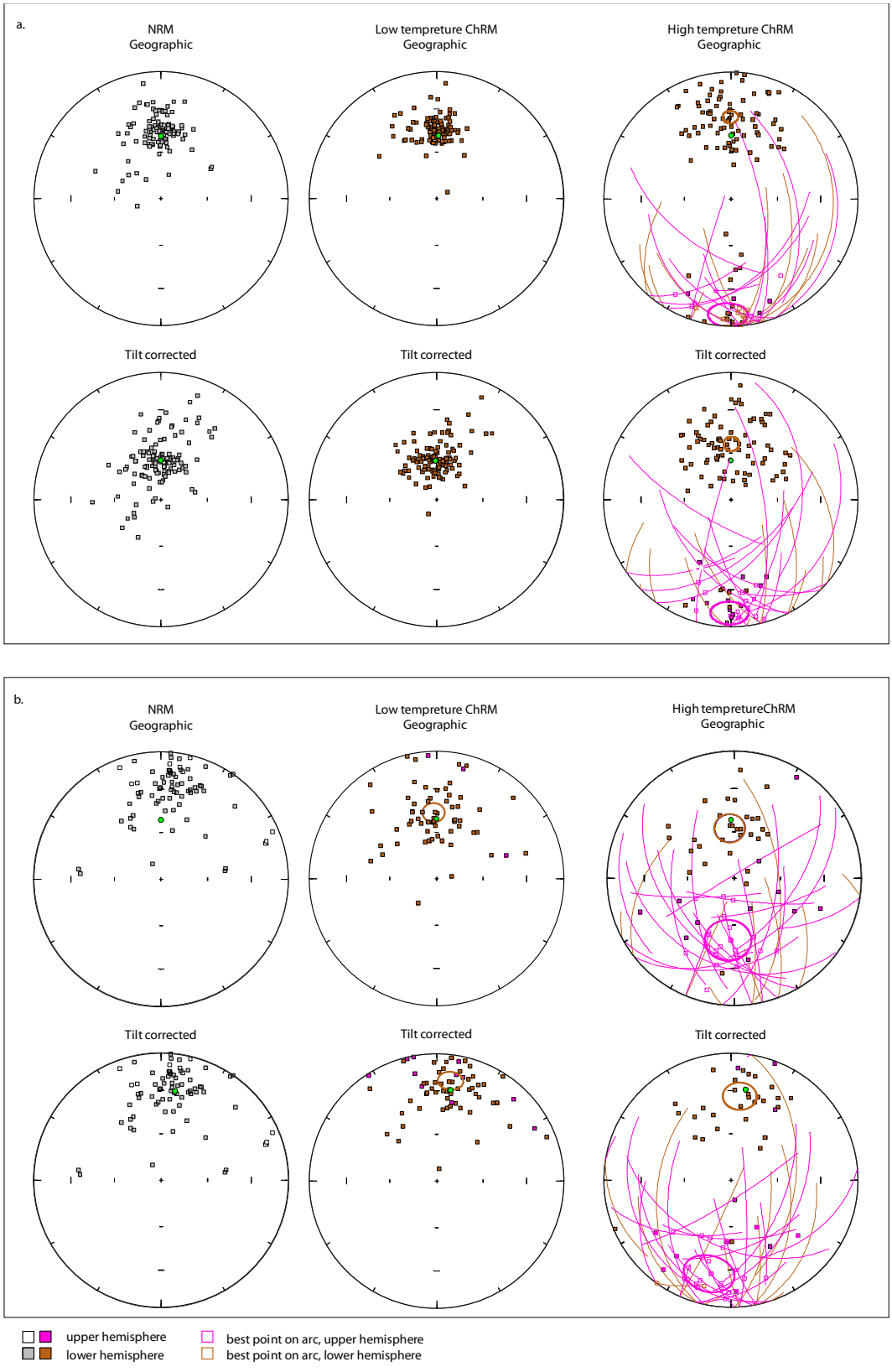

Figure S4: Results of the Principal Component Analysis in equal-area stereographic projections for NRM, Low-T and high-T ChRM for eastern sector, Dehmoord, (a) and western sector, Shalamzar, (b). Low-T components are interpreted to be of recent origin. Two-polarity characteristic directions are shown for normal and reverse directions. Arc constraints for the samples that do not reach the stable endpoints are calculated with the method of McFadden and McElhinny (1988) and are shown with open squares. The present local field is shown with green circle.

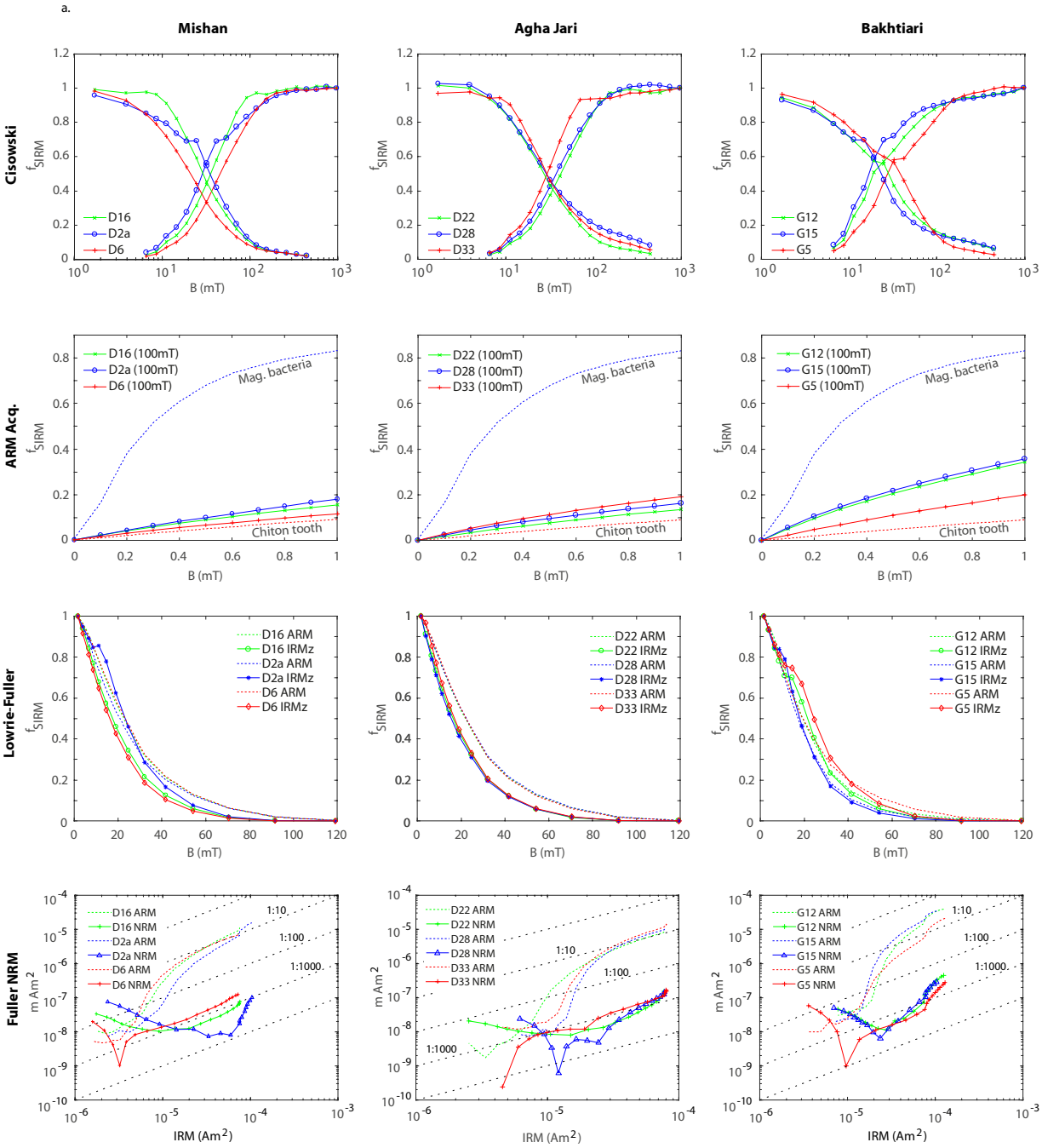

Figure S5: a. Rock magnetic results from the Mishan (column 1), Agha Jari (column 2), and Bakhtiari (column 3) Formations along the Dehmoord section. Locations of the samples are shown in Figure S6a.

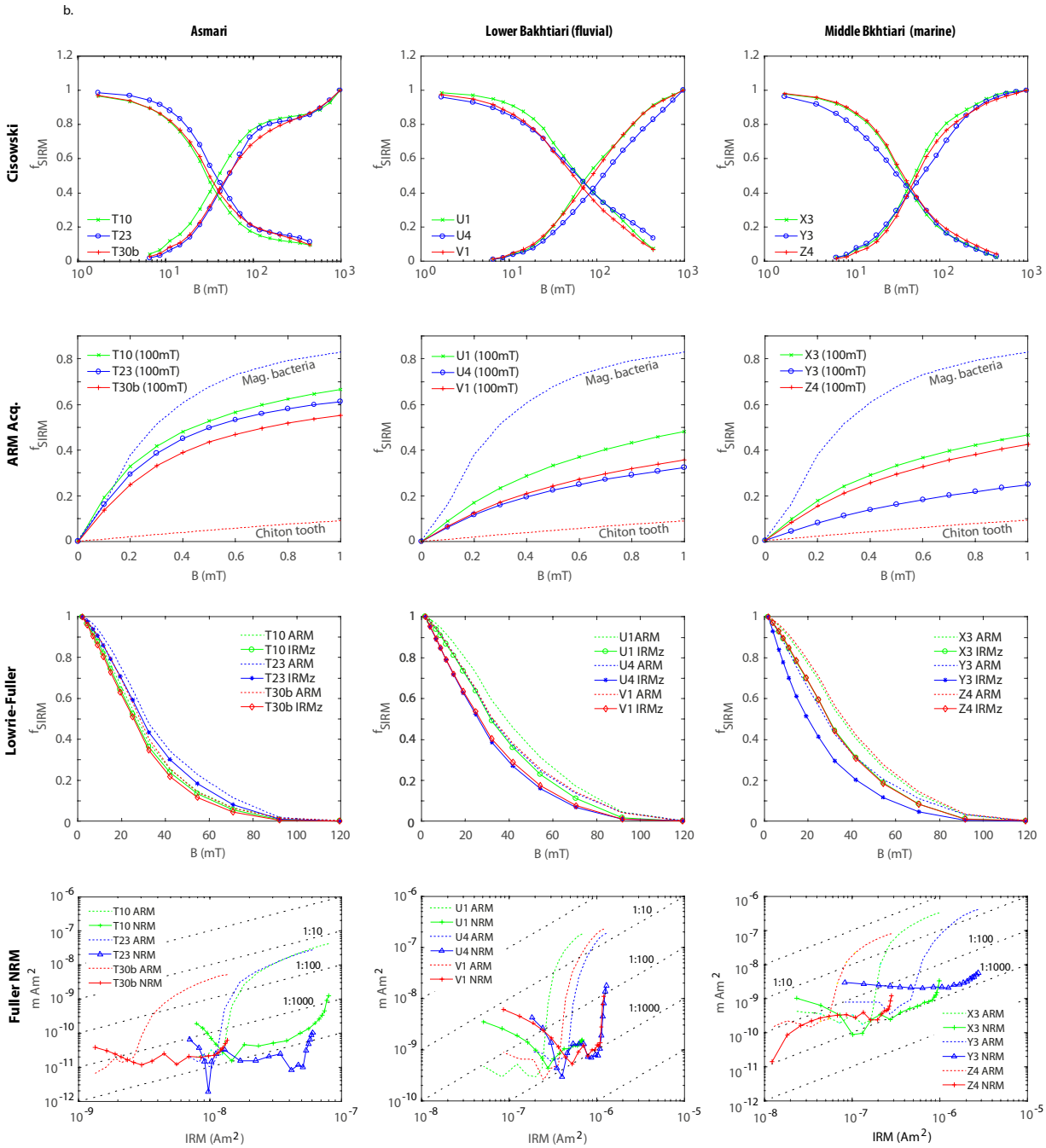

Continued, Figure S5: b. Rock magnetic results from the Asmari (column 1), lower Bakhtiari-fluvial (column 2), and middle Bakhtiari-marine (column 3) outcrops along the Shalamzar section. Locations of the samples are shown in Figure S6b.

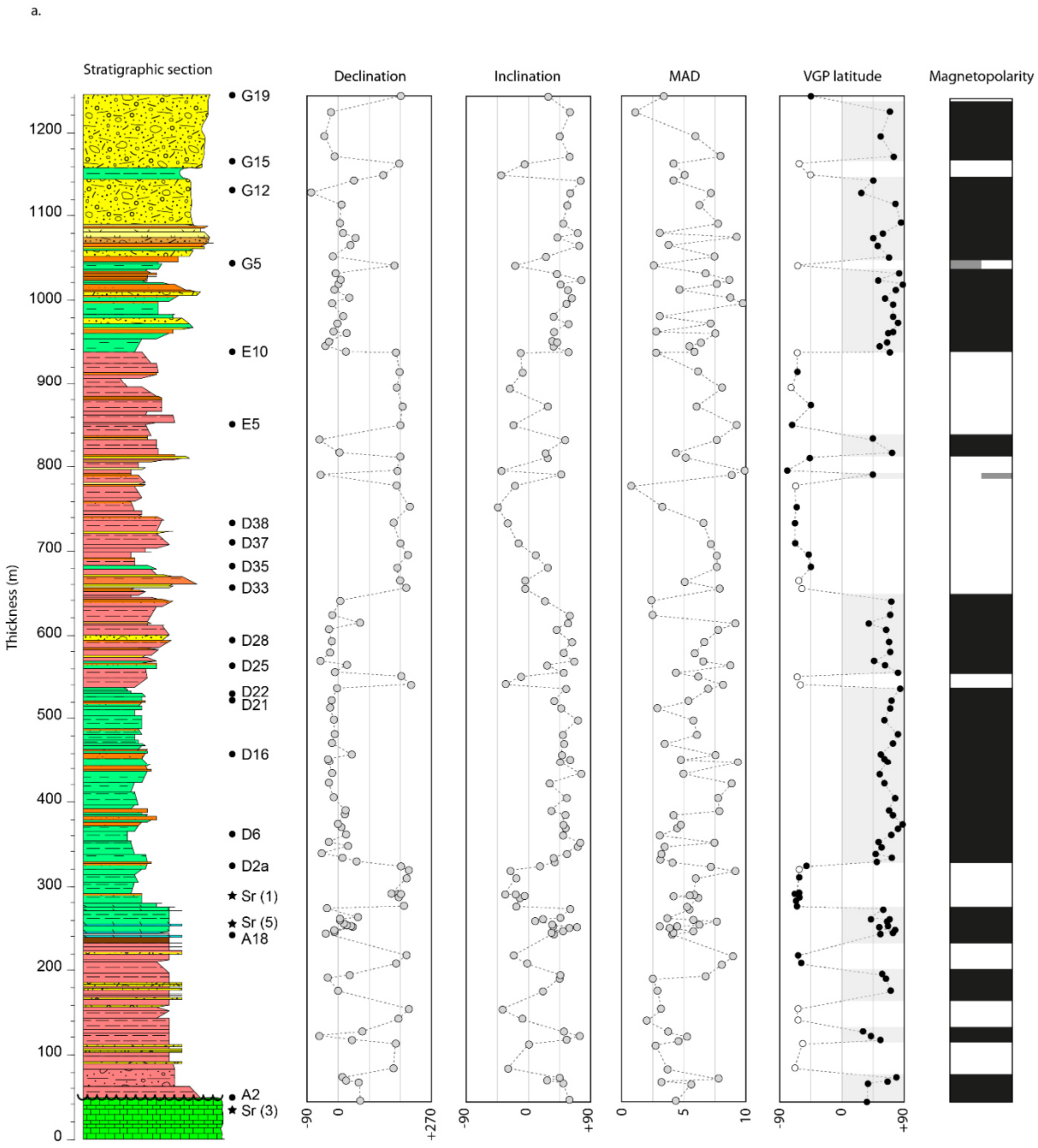

Figure S6. a. Measured stratigraphic column of the Dehmoord section in Neyriz area. Location of the section is shown in Figure 1. Stars and filled circles along the stratigraphic section are the location of strontium isotope and magnetostratigraphic samples. Open circles in the VGP latitude graph shows locations where planes are fitted to the sample, and filled circles represent the line fit.

b.

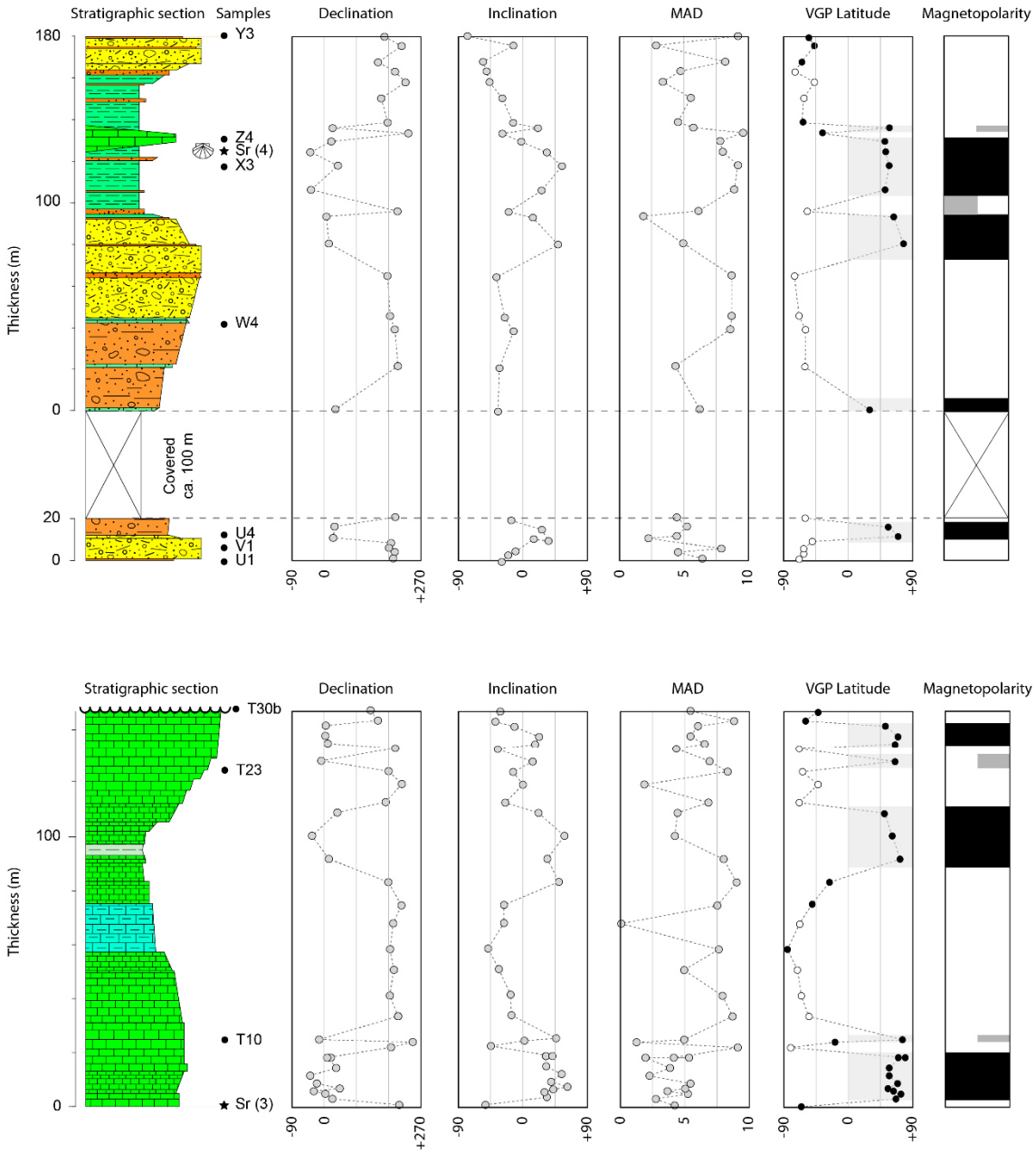

Continued, Figure S6. b. Measured stratigraphic column of the Shalamzar section in the Shahr-e-Kord area. The upper panel shows the Bakhtiari Formation and lower panel represents the Asmari Formation. Lower part of the Bakhtiari Formation is covered.

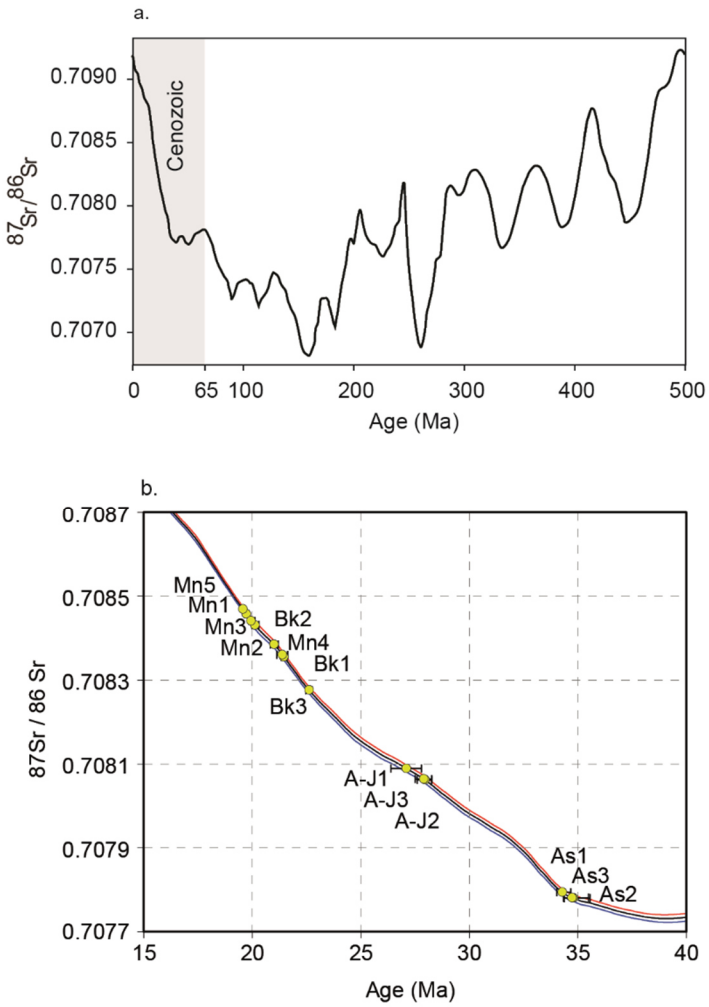

Figure S7: a. Excursion of the $^{87}Sr/^{86}Sr$ strontium isotope ratio in sea water through the Phanerozoic time, (Modified from McArthur and Howarth, 2004). b) Strontium isotope measurements for samples from the Shalamzar and Dehmoord sections are shown with yellow circles. The data are presented in Table 1. As, Asmari; A-J, Asmari-Jahrom; Bk, Bakhtiari; Mn, Mishan.

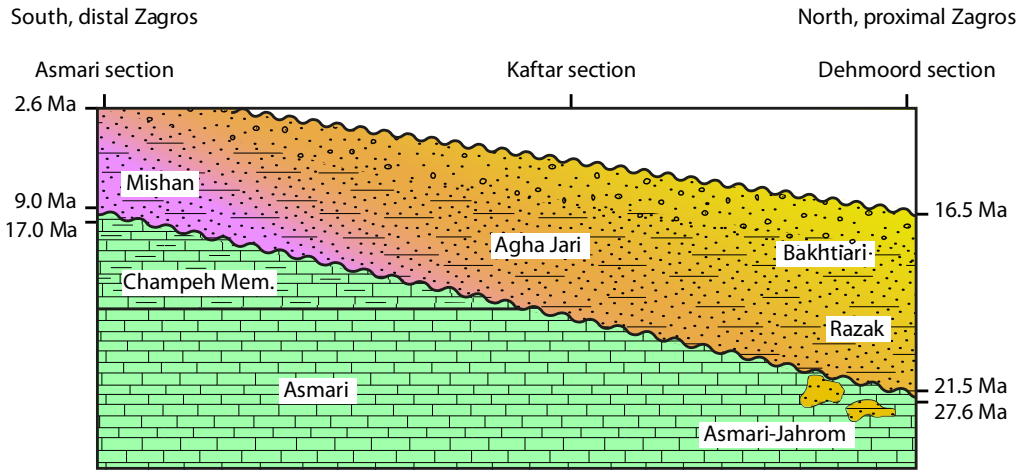

Figure S8: Forebulge unconformity between Asmari-Jahrom and Razak (Detrital equivalent of the Gachsaran) Formations in proximal, and Champeh member of the Gachsaran and Mishan Formations in distal eastern Zagros. For locations see Figures 1 and 7.

References:

Cisowski, S., 1981, Interacting vs. non-interacting single domain behavior in natural and synthetic samples: Physics of the Earth and Planetary Interiors, v. 26, no. 1-2, p. 56-62.

Dekkers, M., 1989, Magnetic properties of natural pyrrhotite. II. High-and low-temperature behaviour of Jrs and TRM as function of grain size: Physics of the Earth and Planetary Interiors, v. 57, no. 3-4, p. 266-283.

Fuller, M., Cisowski, S., Hart, M., Haston, R., Schmidtke, E., and Jarrard, R., 1988, NRM: IRM (s) demagnetization plots; an aid to the interpretation of natural remanent magnetization: Geophysical Research Letters, v. 15, no. 5, p. 518-521.

Johnson, H., Lowrie, W., and Kent, D. V., 1975, Stability of anhysteretic remanent magnetization in fine and coarse magnetite and maghemite particles: Geophysical Journal International, v. 41, no. 1, p. 1-10.

Kirschvink, J., 1980, The least-squares line and plane and the analysis of palaeomagnetic data: Geophysical Journal International, v. 62, no. 3, p. 699-718.

Kirschvink, J. L., Isozaki, Y., Shibuya, H., Otofuji, Y.-i., Raub, T. D., Hilburn, I. A., Kasuya, T., Yokoyama, M., and Bonifacie, M., 2015, Challenging the sensitivity limits of paleomagnetism: magnetostratigraphy of weakly magnetized Guadalupian–Lopingian (Permian) limestone from Kyushu, Japan: Palaeogeography, Palaeoclimatology, Palaeoecology, v. 418, p. 75-89.

Kirschvink, J. L., Kopp, R. E., Raub, T. D., Baumgartner, C. T., and Holt, J. W., 2008, Rapid, precise, and high-sensitivity acquisition of paleomagnetic and rock-magnetic data: Development of a low-noise automatic sample changing system for superconducting rock magnetometers: Geochemistry, Geophysics, Geosystems, v. 9, no. 5.

Lowrie, W., 1990, Identification of ferromagnetic minerals in a rock by coercivity and unblocking temperature properties: Geophysical research letters, v. 17, no. 2, p. 159-162.

McFadden, P., and McElhinny, M., 1988, The combined analysis of remagnetization circles and direct observations in palaeomagnetism: Earth and Planetary Science Letters, v. 87, no. 1, p. 161-172.

Zijderveld, J., 1967, AC demagnetization of rocks: analysis of results: Methods in paleomagnetism, v. 3, p. 254.